NJC

Accepted Manuscript

This is an *Accepted Manuscript*, which has been through the Royal Society of Chemistry peer review process and has been accepted for publication.

Accepted Manuscripts are published online shortly after acceptance, before technical editing, formatting and proof reading. Using this free service, authors can make their results available to the community, in citable form, before we publish the edited article. We will replace this *Accepted Manuscript* with the edited and formatted *Advance Article* as soon as it is available.

You can find more information about *Accepted Manuscripts* in the Information for Authors.

Please note that technical editing may introduce minor changes to the text and/or graphics, which may alter content. The journal's standard Terms & Conditions and the Ethical guidelines still apply. In no event shall the Royal Society of Chemistry be held responsible for any errors or omissions in this *Accepted Manuscript* or any consequences arising from the use of any information it contains.

ROYAL SOCIETY OF CHEMISTRY

www.rsc.org/njc

NJC

RSCPublishing

PAPER

Photophysical properties, aggregation-induced fluorescence in nanoaggregates and cell imaging of 2,5-bisaryl 1,3,4-oxadiazoles

Cite this: DOI: 10.1039/xoxxoooooox

Yongchang Jin, Ying Qian*

Received ooth January 2012,
Accepted ooth January 2012

DOI: 10.1039/xoxxoooooox

www.rsc.org/

Dye-loaded nanoparticles encapsulating four different aggregation-induced emission (AIE) and intramolecular charge transfer (ICT) active chromophores, which had different numbers of carbazole-containing triphenylamine moieties as donors and one 1,3,4-oxadiazole moiety as acceptor, were reported and investigated. Dye-doped amino-group-functionalized silica nanoparticles (Si-NPs), with diameter ~30 nm, maintained the AIE characterized phtophysical properties of the chromophores with high quantum yield up to 0.35 for Oxa-$(BCPA)_1$-doped Si-NPs and the fluorescence emission peaks ranged from 476 nm to 513 nm for the four nanoparticles. Meanwhile, dye-doped Si-NPs had successfully overcome the challenges of poor biocompatibility of AIE materials and could be well dispersed in water, providing an important opportunity to further explore their bioapplications by conjugating the NPs with various biomolecues. The dye-loaded BSA-nanoparticles (BSA-NPs) were applied to cell imaging and showed a better uptake by HeLa cells compared to pure dye NPs, which indicating a promising application for biosensors such as cancer cell detecting.

Introduction

The advanced development of multifunctional nanoparticles provides an exciting opportunity for potential bioapplications such as cell imaging, [1] biosensors, [2] gene delivery, [3] drug carriers [4] and thus has attracted great research attention worldwide in the past few decades. Dye-dopped silica nanoparticles, especially, are one of the most vigorous research fields due to several important merits such as almost precisely controllable size with good monodispersity, simple surface functionalization to meet the specific application requirements, excellent compatibility that could encapsulate different materials in one single particle to realize multifunctional applications, superior optical properties against photobleaching and most importantly, great biocompatibility which will make it possible to explore potential use for dyes with good photophysical properties but incompatible with biosystem. Meanwhile, dyes which could be encapsulated inside nanoparticles should have some advantageous features over traditional aggregation-caused quenching (ACQ) materials because they are usually in aggregated state inside nanoparticles. Aggregation-induced emission (AIE) materials are one of the choices which are widely investigated due to their properties as called. After the AIE phenomena was found,[5] great progress has been made such as using AIE materials to monitor the process proceeding in drug delivery systems[6] or to realize fluorescent cellular tracing[7] and even new fluorescence turn-on mechanism [8] was discovered in addition to AIE. Combination of the development in AIE materials with the nanotechnique will absolutely provide a promising potential in their bioapplications.

Tian [9] synthesised a 9,10-distyrylanthracene-doped folate-functionalized silica nanoparticles with a high fluorescence quantum yield up to 0.20 and showing specific targeting ability to cancer cells over normal cells because the folic acid decorated on the surface of the nanoparticles showed a high binding affinity to the folate receptors overexpressed by many cancer cells. Jung Aa Ko[10] reported metal/dye-doped core-shell silica nanoparticles with diameter of 60 nm containing metal salts and dyes inside one nanoparticle, of which the movement could be easily monitored during the treatment process and thus to realize multiplex detection such as to monitor DNA cleavage. Stefania Biffi [11] developed silica nanoparticles encapsulating two dyes acting as donor–acceptor couple to tune the emission intensity profile into the NIR spectrum by changing the doping ratio of the donor–acceptor couple and could be used for both flow cytometry and in vivo imaging. Gao [12] applied a fluorescence resonance energy transfer system containing oligonucleotide-modified fluorescein isothiocyanate-doped nanoparticles as donors and oligonucleotide-modified gold nanoparticles as acceptors to detect the DNA hybridization with

School of Chemistry and Chemical Engineering, Southeast University, Nanjing, 211189, China. E-mail: yingqian@seu.edu.cn

a detection limit of 3 picomole. Dye-doped nanoparticles have shown great potential in bioapplications, but dyes which not only have excellent photophysical properties, but could also be easily encapsulated inside nanoparticles without any chemical pretreatment are still highly needed.[13]

In this paper, we have reported four different AIE-ICT active chromophores Oxa-$(CPA)_1$, Oxa-$(CPA)_2$, Oxa-$(BCPA)_1$ and Oxa-$(BCPA)_2$, which are fabricated in a D-A or D-A-D manner with one or two carbazole-containing triphenylamine building-blocks as donors while 1,3,4-oxadiazole as the acceptor.[14] Tert-butyl were introduced to the 3,6-positions of carbazole in some cases to improve the solubility of the compounds and enhance the electron-donation.[15] The structures of these compounds are given in scheme 1. CPA/BCPA represents the two important intermediates with or without tert-butyl, respectively. Oxa-$(CPA)_1$ and Oxa-$(BCPA)_1$ are of one-donor-containing structure while Oxa-$(CPA)_2$ and Oxa-$(BCPA)_2$ are of two-donor-containing structure, respectively. Photophysical properties of the chromophores in different solvents and aggregated states were investigated. Indeed, both positive solvatochromism and excellent performance in solid state characterized by AIE effect were observed. Amino-group-functionalized silica nanoparticles (Si-NPs) encapsulating the aggregated chromophores and dye-loaded BSA nanoparticles were prepared to explore potential bioapplications. Photophysical properties of Si-NPs are discussed and dye-loaded BSA nanoparticles were successfully applied to cell imaging.

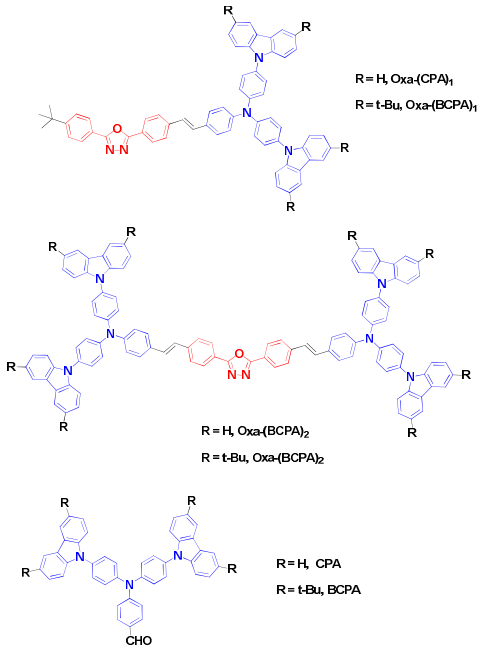

Scheme 1 Chemical structures of chromophores Oxa-$(CPA)_n$, Oxa-(BCPA)n (n=1,2) and CPA/BCPA. When n=1, the chromophores have an asymmetric structure with only one building block of CPA/BCPA and while n=2, a symmetrical structure is obtained. CPA/BCPA represents the important intermediates or building blocks in different cases.

Experimental

General

N,N-di(4-iodophenyl) amino benzaldehyde, [[4-[5-(4-tert-butylphenyl)-1,3,4-oxadiazol-2-yl]phenyl]methyl] triphenylphosphonium bromide , 2,5-bis(4-methylphenyl)-1,3,4-oxadiazole triphenylphosphonium bromide, 3,6-Di-tert-butyl-9H-carbazole were synthesised by our laboratory using the known literature procedure[16] and identified by ^{1}H NMR and melting point analysis. Solvents were purified and dried using standard protocols. All other chemical reagents were obtained commercially and were used as received without further purification. 3-aminopropyltriethoxysilane (APTES, Sinopharm Chemical Reagent Co., Ltd, Shanghai, China), Aerosol OT (AOT, Aladdin Industrial Co., Shanghai, China), triethoxyvinylsilane (VTES, Aladdin Industrial Co., Shanghai, China).

Chemical structures were confirmed by NMR analysis. ^{1}H NMR measurements were determined with a Bruker 500 MHz spectrometer or Bruker 300 MHz spectrometer, with TMS (tetramethyl silane) as the internal standard. ^{13}C NMR measurements were determined with a Bruker 300 MHz spectrometer.

UV-visible absorption spectra were determined on a Shimadu UV-3600 spectrophotometer. Fluorescence spectra were measured on an HORIBA FL-4 max spectrometer. The melting points were measured on a Microscopic Melting Point Meter X-4. The cell imaging equipment used in our experiment were Upright Fluorescence Microscope (Imager A1) provide by ZEISS, Germany.

Synthesis

4-N,N-Bis[4-(3,-6-di-tert-butylcarbazol-9-yl)phenyl]-amino-benzaldehyde (BCPA). Yellow solid. Yield 80%. m.p. >300℃. A mixture of N,N-di(4-iodophenyl) amino benzaldehyde (5.0 g, 9.5 mmol), 3,6-Di-tert-butyl-9H-carbazole (5.8 g, 20.9 mmol), CuI (0.72 g, 3.78 mmol), 1,10-phenanthroline (1.5 g, 8.3 mmol), and K_2CO_3 (3.5 g, 20.9 mmol) in DMF (50 mL) was heated to 160 ℃ under nitrogen for 24 h. After cooling to room temperature, the reaction mixture was poured into water (100 mL). The precipitate was filtered and dried. Further purification was performed by column chromatography to afford the pure product. ^{1}H NMR (300 MHz, $CDCl_3$) δ: 9.93 (s, 1H), 8.18 (s, 4H), 7.87 (d, J=8.52 Hz, 2H), 7.63 (d, J=8.49 Hz, 4H), 7.54–7.45 (m, 12H), 7.31(d, J=8.19 Hz, 2H), 1.50 (s, 36H).

4-N,N-Bis[4-(carbazol-9-yl)phenyl]-amino-benzaldehyde (CPA). Yellow solid. Yield 89%. m.p. 287-289 ℃. The synthetic procedure of CPA was similar to that of BCPA. ^{1}H NMR (300 MHz, CDCl3) δ: 9.91 (s, 1H), 8.17 (d, J=7.74 Hz, 4H), 7.86 (d, J=8.64 Hz, 2H), 7.62 (d, J=8.67 Hz, 4H), 7.52–7.42 (m, 12H), 7.33–7.28 (m, 6H).

2-(4-tert-butylphenyl)-5-{4-[2-[4-N,N-bis-(4-carbazol-9-yl-phenyl)-amino-phenyl]vinyl]phenyl}-1,3,4-oxadizole [Oxa-

(CPA)$_1$]. Yellow solid. Yield 66%. m.p. 293-295℃. [[4-[5-(4-tert-butylphenyl)-1,3,4-oxadiazol-2-yl]phenyl]methyl] triphenylphosphonium bromide (1 g, 1.58 mmol) was dissolved in 20 mL THF at 0℃. A solution of sodium hydride (0.06 g, 2.68 mmol) in 5 mL THF was added under nitrogen. After the mixture was stirred for 1 h, 4-N,N-Bis[4-(carbazol-9-yl)phenyl]-amino-benzaldehyde (1.05 g, 1.74 mmol) in 20 mL THF was added dropwise to the reaction mixture for 0.5 h. Then the mixture was stirred at 80℃ for 2 h. After cooling to room temperature, the reaction was quenched with 100 mL water. The mixture was filtered and dried. The crude product was purified by column chromatography on silica gel to afford the pure product. ^{1}H NMR (500 MHz, CDCl3) δ: 8.18 (d, J=7.70 Hz, 4H), 8.15 (d, J=7.35 Hz, 2H), 8.09 (d, J=7.00 Hz, 2H),7.69 (d, J=7.25 Hz, 2H), 7.59-7.56 (m, 4H), 7.55-7.53 (m, 4H), 7.51 (d, J=8.05 Hz, 4H), 7.47-7.44 (m, 8H), 7.30-7.33 (m, 6H), 7.27 (d, J=15.05 Hz, 1H), 7.14 (d, J=15.95 Hz, 1H), 1.39 (s, 9H). ^{13}C NMR (300 MHz, $CDCl_3$) δ: 167.20, 166.90, 157.95, 149.88, 148.89, 143.58, 143.37, 135.32, 134.72, 132.79, 130.75, 130.70, 129.89, 129.48, 129.40, 129.13, 128.67, 128.53, 127.88, 127.07, 125.95, 125.21, 123.75, 122.95, 122.53, 112.39, 37.70, 33.74.

2,5-di-{4-[2-[4-N,N-bis-(4-carbazol-9-yl-phenyl)-amino-phenyl]vinyl]phenyl}-1,3,4-oxadizole [Oxa-(CPA)$_2$]. Yellow solid. Yield 54%. m.p. 262-264℃. The synthetic procedure of Chromophore Oxa-$(CPA)_2$ was similar to that of Chromophore Oxa-$(CPA)_1$. 1H NMR (500 MHz, $CDCl_3$) δ: 8.17-8.14 (m, 12H), 7.68 (d, J=8.30 Hz, 4H),7.58 (d, J=8.50 Hz, 4H),7.54 (d, J=8.65 Hz, 8H),7.50 (d, J=8.15 Hz, 8H),7.46-7.43 (m, 16H),7.33-7.29 (m, 12H),7.27 (d, J=16.30 Hz, 2H),7.14 (d, J=16.25 Hz, 2H). ^{13}C NMR (300 MHz, $CDCl_3$) δ: 164.45, 147.33, 146.31, 140.99, 132.75, 132.10, 130.28, 128.17, 128.12, 127.34, 126.92, 126.51, 125.94, 125.31, 124.47, 123.37, 122.53, 120.37, 119.95, 114.61, 109.80.

2-(4-tert-butylphenyl)-5-{4-[2-[4-N,N-bis-[4-(3,6-di-tert-butylcarbazol-9-yl)phenyl]-amino-phenyl]vinyl]phenyl}-1,3,4-oxadizole [Oxa-(BCPA)$_1$]. Yellow solid. Yield 50%. m.p. 264-266℃. The synthetic procedure of Chromophore Oxa-$(BCPA)_1$ was similar to that of Chromophore Oxa-$(CPA)_1$. ^{1}H NMR (300 MHz, CDCl3) δ: 8.20 (s, 4H), 8.19 (d, J=9.43 Hz, 2H), 8.14 (d, J=8.37 Hz, 2H), 7.72 (d, J=8.25 Hz, 2H), 7.61-7.58 (m, 4H), 7.58-7.55 (m, 4H), 7.55-7.53 (m, 4H),7.49-7.44 (m, 8H), 7.36 (d, J=8.34 Hz, 2H),7.32 (d, J=12.42 Hz, 1H),7.17 (d, J=16.20 Hz, 1H), 1.53 (s, 36H), 1.42 (s, 9H). ^{13}C NMR (300 MHz, $CDCl_3$) δ: 167.19, 166.93, 157.93, 150.05, 148.49, 145.45, 143.44, 141.96, 135.92, 134.42, 132.87, 130.65, 130.34, 129.88, 129.46, 129.41, 128.95, 128.67, 127.93, 126.78, 126.20, 125.95, 125.17, 123.79, 118.88, 111.85, 37.71, 37.36, 34.65, 33.75.

2,5-di-{4-[2-[4-N,N-bis-[4-(3,6-di-tert-butylcarbazol-9-yl)phenyl]-amino-phenyl]vinyl]phenyl}-1,3,4-oxadizole [Oxa-(BCPA)2]. Yellow solid. Yield 53%. m.p. 291-293℃. The synthetic procedure of Oxa-$(BCPA)_2$ was similar to that of Chromophore Oxa-$(CPA)_1$. ^{1}H NMR (300 MHz, CDCl3) δ: 8.20-8.17 (m, 12H), 7.72 (d, J=8.22 Hz, 4H),7.61 (d, J=11.28 Hz, 4H),7.57 (d, J=7.44 Hz, 8H), 7.54-7.52 (m, 8H),7.48-7.44 (m, 16H), 7.35 (d, J=8.52 Hz, 4H),7.32 (d, J=14.34 Hz, 2H),7.17 (d, J=16.20 Hz, 2H), 1.52 (s, 72H). ^{13}C NMR (300 MHz, $CDCl_3$) δ: 167.04, 150.07, 148.48, 145.46, 143.54, 141.96, 135.93, 134.39, 132.94, 130.65, 130.34, 129.93, 129.49, 128.92, 127.95, 126.76, 126.20, 125.95, 125.06, 118.88, 111.85, 37.35, 34.65.

Preparation of dye-encapsulated amine-functionalized silica nanoparticles

To a clear solution of surfactant AOT (0.44 g) dissolved in deionized water (20 mL) was added 0.8 mL cosurfactant 1-butanol under sonication at 0 ℃ to form oil-in-water microemulsion system. DMF (60 μL) solution containing Oxa-$(CPA)_n$ or Oxa-$(BCPA)_n$ (10 mM) was dropped into the mixture. After sonicating for 3 min, 0.2 mL VTES was added and the reaction mixture was stirred for 8 h. APTES (20 μL) was added and the mixture was further stirred at room temperature for 24 h. After the formation of nanoparticles, the unreacted starting materials were removed by dialyzing the solution against deionized water in a 8-14 KDa cutoff cellulose membrane for 72 h. The dialyzed solution was then stored at 5 ℃ for later use.

Preparation of dye-loaded BSA nanoparticles

BSA (0.1300 g) was dissolved in deionized water (50 mL) and a solution of THF (80 mL) containing 0.0013 g dye was added dropwise under sonication. Then 100 μL glutaraldehyde solution (25%) was added at room temperature and the mixture was stirred for 4 h. The THF was removed by rotary evaporation and stored at 5 ℃ for later use.

Cell culture

HeLa cells (human cancer cell lines) were grown in Dulbecco minimum essential media (DMEM) with 10% fetal bovine serum (FBS), 1% penicillin, and 1% amphotericin B. Before the treatment, the cell were plated in 24-well plates and incubated for 24 h. Then different nanoparticles were added at a concentration equal to 1.3×10^{-6} g/L of pure dyes and incubated for 4 hours at 37 ℃ with 5% CO_2. Then the cells were washed twice with PBS and imaged with a Fluorescence Microscopy.

Cytotoxicity of dye-loaded BSA-NPs

The cytotoxicity of the BSA-NPs against HeLa cells was assessed by MTT assay using the known literature procedure.[17]

Results and discussion

Synthesis of the chromophores with different number of building blocks

All the four final compounds, Oxa-$(CPA)_n$, Oxa-(BCPA)n (n=1,2), were synthesised through two main reactions after obtaining of the important intermediates, which were N,N-di(4-iodophenyl) amino benzaldehyde, 3,6-Di-tert-butyl-9H-carbazole, [[4-[5-(4-tert-butylphenyl)-1,3,4-oxadiazol-2-yl] phenyl]methyl]triphenylphosphonium bromide and 2,5-bis(4-methylphenyl)-1,3,4-oxadiazole triphenylphosphonium bromide. Ullmann reaction connected the carbazol-9-yl (with or without tert-butyl substitution at 3,6-positions) to N,N-di(4-iodophenyl) amino benzaldehyde at the sites of iodine atoms to generate CPA/BCPA with good yield (>80%). Then CPA/BCPA reacted with one/two-branched compounds: [[4-[5-(4-tert-butylphenyl)-1,3,4-oxadiazol-2-yl]phenyl]methyl] triphenylphosphonium bromide or 2,5-bis(4-methylphenyl)-1,3,4-oxadiazole triphenylphosphonium bromide by Wittig reaction and the final chromophores were obtained with a middle yield (>50%). All of the final compounds were confirmed by ^{1}H NMR and ^{13}C NMR. The synthetic routes of the chromophores are shown in Scheme 2, taking Oxa-$(BCPA)_2$ as an example and the rest synthetic routes are provided in the supplementary information.

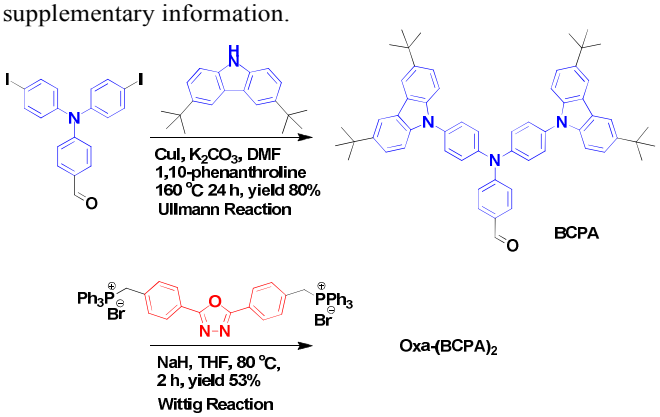

Scheme 2 Synthetic routes of target chromophores Oxa-$(BCPA)_2$

Photophysical properties of 2,5-bisaryl-1,3,4-oxadiazoles

The CPA/BCPA and four 2,5-bisaryl-1,3,4-oxadiazoles can be devided into two groups by structures without (group 1: CPA, Oxa-$(CPA)_1$ and Oxa-$(CPA)_2$) or with (group 2: BCPA, Oxa-$(BCPA)_1$ and Oxa-$(BCPA)_2$) tert-butyls on the 3,6-positions of carbazoles. The normalized fluorescence spectra of the four 2,5-bisaryl-1,3,4-oxadiazoles in solid state was shown in Fig. 1a. The maximum emission peaks of the four chromophores were from 494 nm to 523 nm （Table1）. Obvious bathochromic shift was observed when the one-donor-containing compounds changed into two-donor-containing compounds, for example, 494 nm for Oxa-$(CPA)_1$ and 523 nm for Oxa-$(CPA)_2$. The fluorescence pictures of solid powder excited at 365 nm are also presented in the inset. The CIE chromaticity coordinate of the four chromophores was depicted in Fig. 1b. The CIE chromaticity coordinate values of Oxa-$(CPA)_1$, Oxa-$(CPA)_2$, Oxa-$(BCPA)_1$ and Oxa-$(BCPA)_2$ were calculated to be (0.21, 0.49), (0.32, 0.62), (0.18, 0.51) and (0.25, 0.61), respectively. An obvious change from green to yellowish green is observed when the one-donor-containing compounds changed into two-donor-containing compounds.

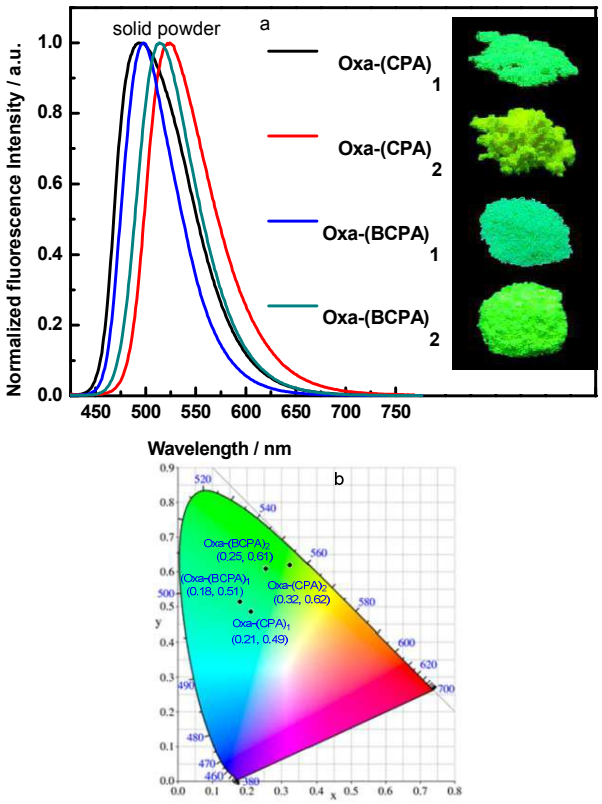

Fig. 1 The normalized fluorescence spectra of the 2,5-bisaryl-1,3,4-oxadiazoles in solid state excited at 400 nm (a) and the inset presented the fluorescence pictures of solid powder excited at 365 nm; the CIE chromaticity coordinate of the four chromophores(b).

All the two groups of compounds are soluble in common organic solvents such as CH_2Cl_2, THF and DMF. Fig. 2 (a, b) shows the absorption and emission spectra of them in THF solution. Two major absorption bands located at 300-350 and 350-475 nm are observed. The former is ascribed to localized π-π* transition of aromatic moieties in the molecular while the latter is of ICT character.[18] In changing from CPA, Oxa-$(CPA)_1$ to Oxa-$(CPA)_2$ (Group 1, Fig. 2a), the maximum absorption peaks within 300-350 nm almost remain unchanged but an obvious bathochromic shift from 365 nm, 396 nm to 407 nm is spotted for the ICT band within 350-475 nm. The ratio of molar extinction coefficient ε_{max} [Oxa-$(CPA)_2$]:ε_{max} [Oxa-$(CPA)_1$] calculated from the ICT band is 10.1:1.0. Excited at the absorption maximum, CPA, Oxa-$(CPA)_1$ and Oxa-$(CPA)_2$ have single emission peaks locating at 498 nm, 504 nm and 508 nm, respectively, and the fluorescence intensity is increased from CPA, Oxa-$(CPA)_1$ to Oxa-$(CPA)_2$ by a ratio of 1.0:4.1:7.8. The same trend is spotted in group 2 (Fig. 2b), with bathochromic shifts in fluorescence spectra (≈10 nm) compared to group 1, which is resulted from the electron-donating ability of tert-butyl. The data is provided in Table 1. It is obvious that the additional carbazole-containing triphenylamine chromophore moiety has largely affected the optical property of the 2,5-bisaryl-1,3,4-oxadiazoles, showing increased molar extinction coefficient and fluorescence intensity.

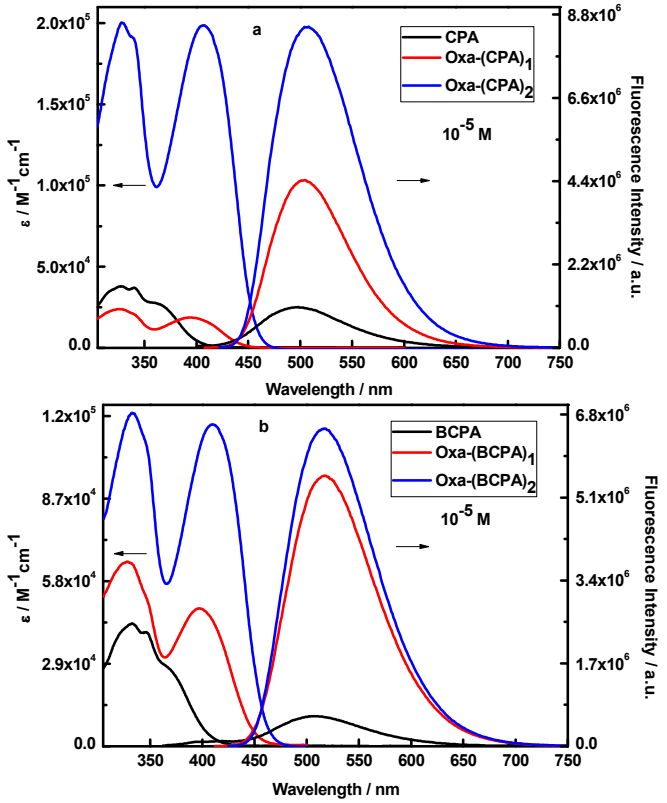

Fig. 2 Absorption and emission spectra of CPA, Oxa-$(CPA)_1$, Oxa-$(CPA)_2$ (a) and BCPA, Oxa-$(BCPA)_1$, Oxa-$(BCPA)_2$ (b) in THF with a concentration of 10^{-5} M.

The solvatochromism behaviour of the 2,5-bisaryl-1,3,4-oxadiazoles was investigated. As seen in Fig. 3, taking Oxa-$(CPA)_1$ as an example, the emission spectra of the chromophore undergo changes induced by the solvents owing varying polarities. In stark contrast to a slightly positive solvatochromism effect in the absorption properties, a remarkable change in the emission maximums (Fig. 3a) ranging from 497 nm (CCl_3) to 546 nm (DMF) indicates that ICT transitions are facilitated in more polar solvents such as DMF and ICT process probably occurs in the excited state of the molecule. Meanwhile, a decreasing in fluorescence intensity is also observed in highly polar solvents , with a ratio of 3.8(CCl_3):1(DMF) for example, due to the fast interconversion from the high emissive local excited (LE) state to the low emissive ICT state reported by many groups.[19]

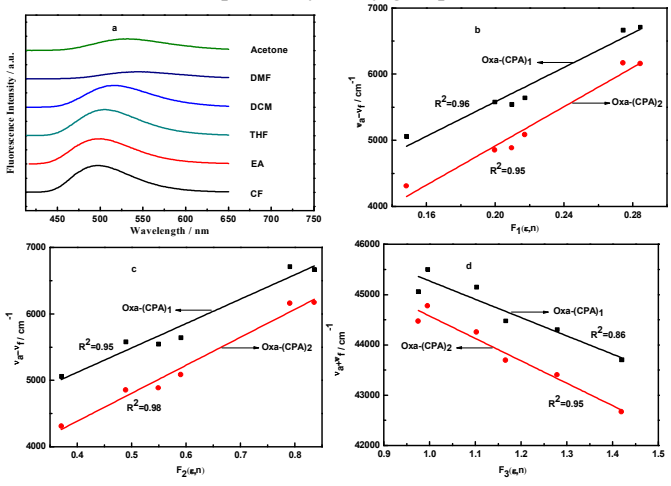

Fig. 3 The emission (a) spectra of Oxa-$(CPA)_1$ in different solvents at the concentration of 10^{-5} M and the linear plots of the Lippert's equation (b), Bakshiev's equation (c) and Kawski–Chamma–Viallet's equation (d) for Oxa-$(CPA)_1$ and Oxa-$(CPA)_2$, the calculation processes and definition of the functions are performed according to the literature.[15]

Three equations, Lippert's equation, Bakshiev's equation, Kawski–Chamma–Viallet's equation are often used to estimate the dipole moment change of the molecular when excited.[20] The linear plots of the three equations are given in Fig. 3 (b, c, d), from good to excellent R^2 value can be observed and the detailed information is listed in Table 1. From the calculation results, large dipole moment difference Δμ ranging from 9.38 D to 13.25 D are obtained, indicating a strong ICT effect occurs during the excitation and emission process and the excited state of the molecule possess an increased dipole moment compared than that of the ground state (Table 1). The electron distribution in the molecular were simulated and the results are provide in Fig. 4a, the electron densities are largely located on the donor in HOMO while in LUMO the electron densities mostly located on the acceptor through the π-bridge. From comparing the electron distribution condition in the HOMO and LUMO levels, an obvious ICT process is observed from the electron-rich region (donor) to the electron-poor region (acceptor) as depicted in Fig. 4b.

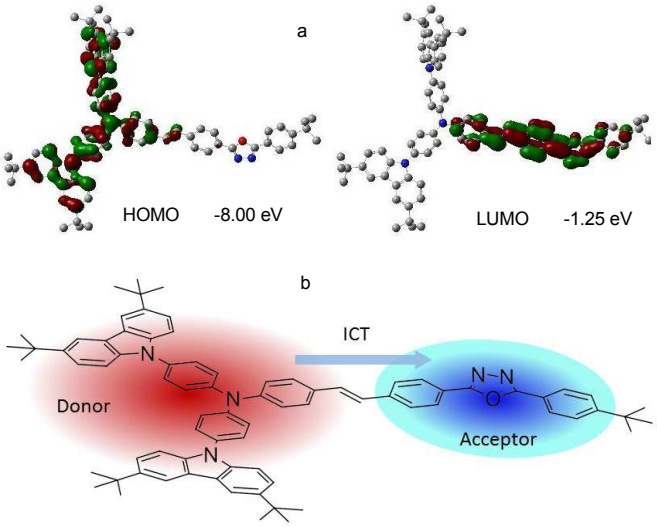

Fig. 4 Frontier molecular orbitals of Oxa-$(BCPA)_1$ (a) and model picture of ICT process from the electron-rich region (donor) to the electron-poor region(acceptor) (b).

Table 1 Photophysical properties of the four chromophores **Oxa-(CPA)n** and **Oxa-$(BCPA)_n$** (n=1,2)

	λ_{em} (nm) (Solid)	λ_{abs} (nm) (THF)	ε_{max} ($M^{-1}cm^{-1}$) (THF)	λ_{em} (nm) (THF)	Stoke's shifts (cm^{-1}) (THF)	Δμ (D)
Oxa-$(CPA)_1$	494	396	1.98×10^4	504	5547	9.38
Oxa-$(CPA)_2$	523	407	2.00×10^5	508	4885	11.73
Oxa-$(BCPA)_1$	498	398	4.87×10^4	517	5696	11.10
Oxa-$(BCPA)_2$	515	410	1.14×10^5	518	5032	13.25

* λ_{abs} UV absorption maximum; λ_{em} fluorescence emission maximum; ε_{max} maximum molar extinction coefficient; $\Delta\mu = \mu_e - \mu_g$, μ_e dipole moment of excited state, μ_g dipole moment of ground state.

From the discussion above, the two groups of chromophores indicated structure-related emission in solid states, showing an obvious change from green to yellowish green when the one-donor-containing compounds changed into two-donor-containing compounds. Solvatochromism effect, a sign of ICT, was also observed due to the D-A configuration of the chromophores. Thus it is necessary to further investigate the photophysical properties of the chromophores in different aggregated states to explore the potential bioapplications.

Aggregation-induced fluorescence in nano-aggregates and cell imaging

All the chromophores are insoluble in water and the dispersion system of nano-aggregates was obtained by gradual addition of water into THF with different ratios. As seen in Fig. 5a, when the water fraction f_W < 60% for Oxa-$(CPA)_1$, the absorption peaks almost remain unchanged. However, with more water added, remarkable changes were observed which can be attributed to the aggregation of the chromophore molecules. In spite of this, the water/THF system remain homogenous without obvious precipitates, indicating that aggregates are probably at nanoscale sizes which can also be proved by the level-off tail stretched into the longer wavelength region in absorption spectra.[21] The emission spectra were presented in Fig. 5 (b, c). The V-profiled fluorescence intensity plots (Fig. 5c) obviously indicated a synergic effect of two different mechanisms, ICT and AIE effect. When the water fraction increased from 0 to 50%, the emission peaks bathochromic shifted from 501 nm to 533 nm and the fluorescence intensity decreased dramatically from quantum yield (Φ_f) up to 0.55 in THF and to a very low value at the water fraction of 50%. This can be attributed to an enhanced extent of ICT process when the more polar solvent water was added. In a less polar system (THF), the emission mostly comes from local excited (LE) state which is high in fluorescence intensity and short in emission peak, while with the polarity of the system increasing, ICT process is facilitated and LE state is substituted by ICT state and bathochromic-shifted emission accompanied by decreasing in emission intensity occurs.[22] But with the more water added (f_W > 50%), the solubility of the mixture solvent decreased and nano-aggregates started to form, ICT was eliminated and AIE effect became a dominated factor.[23] Thus a blue-shifted wavelength (from 533 nm to 504 nm) and increased fluorescence intensity (Φ_f =0.28, f_W = 80%) were observed due to a decreasing in the polarity of local environment and the restricted intramolecular torsion in aggregated state. The detailed quantum yield in mixed solvent of water and THF system are presented in Table 2. Fig. 6 shows the fluorescence pictures of Oxa-$(BCPA)_1$ (a) and Oxa-$(BCPA)_2$ (b) in mixed solvent of water and THF system with different water fractions at concentrations of 10^{-5} M excited at 365 nm.

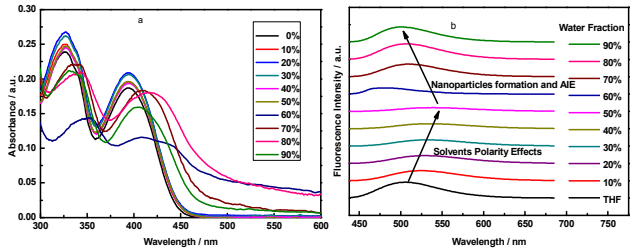

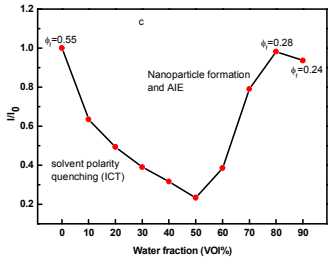

Fig. 5 Absorption (a) and fluorescence spectra (b) of 10^{-5} M Oxa-$(CPA)_1$ in the mixed solvent of water and THF system with different water fractions and corresponding changes in PL peak intensities(I/I_0, I_0= PL intensity in pure THF solution) (c).

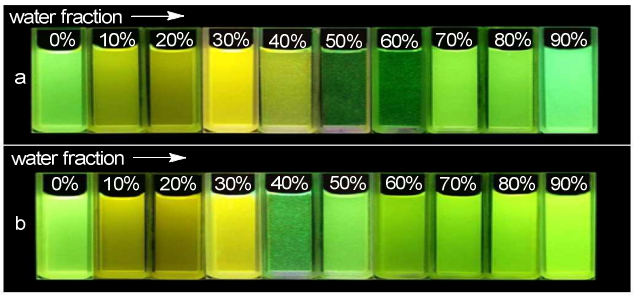

Fig. 6 The fluorescence pictures of Oxa-$(BCPA)_1$ (a) and Oxa-$(BCPA)_2$ (b) in mixed solvent of water and THF system with different water fractions at concentrations of 10^{-5} M excited at 365 nm.

From the discussion above, it can be concluded that all the four chromophores are AIE-ICT active with good photophysical properties in aggregated state with quantum yield even up to 53% for Oxa-$(BCPA)_1$ in mixed solvent of water and THF system with water fraction of 90%. Thus it is necessary to further explored for potential bioapplications.

The main obstacle is that they are incompatible to aqueous biological systems because of poor solubility in water,[24] which is a common problem that largely limits their bioapplications. To overcome these limitations, we have synthesised two kinds of nanoparticles with different structural features aiming at various functions such as cell imaging, biosensor, gene delivery and drug carriers. Amino-group-functionalized Si-NPs were synthesized as the first step towards the promising applications in cell imaging or bioprobes because that amino groups can be easily modified in the next step by biomolecules which would be able to, for instance, target specifically the cancer cells or detect DNA hybridization.[25]

The model structure of the Si-NPs is presented in Fig. 7(left). It is consisted by two parts: (1) the core made of aggregatied chromophore molecules and (2) the silica shell whose internal surface was modified by vinyl that would create a non-polar environment for organic chromophores while the outside surface was decarated with amino groups which would provide bonding sites for biomolecules. TEM image of the dye-doped Si-NPs is shown in Fig.6(right). The average particle size of the Si-NPs indicated by the TEM image is 30 nm.

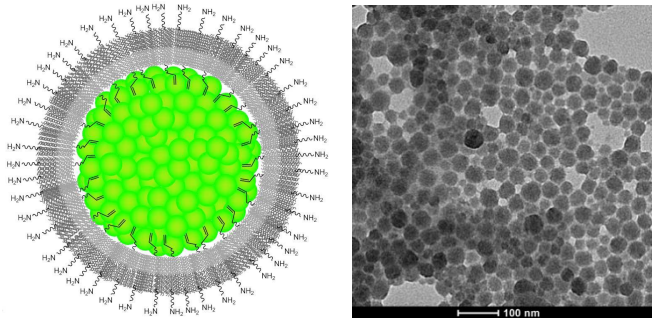

Fig. 7 Model structure (left) and TEM picture (right) of Oxa-$(BCPA)_2$ doped and amino-group-functionalized nanoparticles with average diameter of 30 nm.

The absorbance and fluorescence spectra of the dye-doped Si-NPs were investigated to assess the photophysical properties of the chromophores when encapsulated in nanoparticles. All the four Si-NPs can be well dispersed in water while the good inherent photophysical properties of the pure dyes were maintained as presented in Fig. 8 and Table 2. The absorption peaks of dye-doped Si-NPs were at 411, 414, 419, 420 nm while the emission peaks were at 500, 507, 476, 513 nm, showing a Stoke's shifts of 89, 93, 57, 93 nm respectively for Oxa-$(CPA)_1$, Oxa-$(CPA)_2$, Oxa-$(BCPA)_1$ and Oxa-$(BCPA)_2$. Taking Oxa-$(BCPA)_2$ as an example to compare the emission behavior of the chromophores in different states, the emission peaks of which located at 518 nm in pure THF, 542 nm in mixed solvent of water and THF system with water fraction of 20%, 518 nm when the water fraction is 50%, 509 nm when the water fraction is 90% and 513 nm if Oxa-$(BCPA)_2$ was encapsulated in Si-NPs dispersed in water. It was obvious that the emission peaks of dyes encapsulated inside the silica shell were similar to that of which was in low polar solvent THF or aggregated particles dispersed in higher water fraction and different from in mix-solvents with lower water fractions such as 20%. Meanwhile, the quantum yield of Oxa-$(BCPA)_1$ is up to 35% and Oxa-$(BCPA)_2$ is up to 23%, respectively. Thus it could be concluded that the excellent photophysical properties of the chromophores in solid states were maintained in the Si-NPs while the potential bioapplications based on the Si-NPs could be further explored.[26]

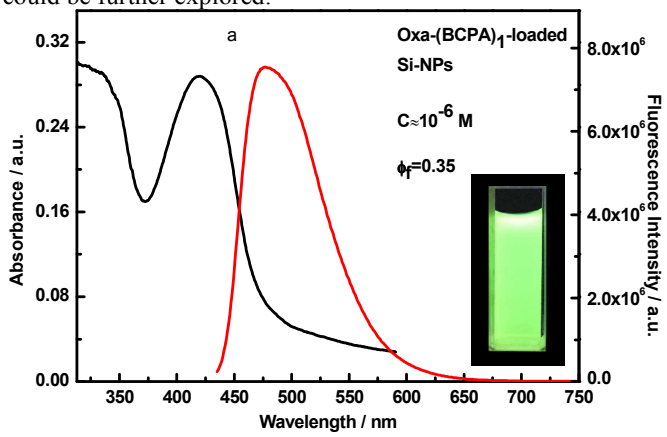

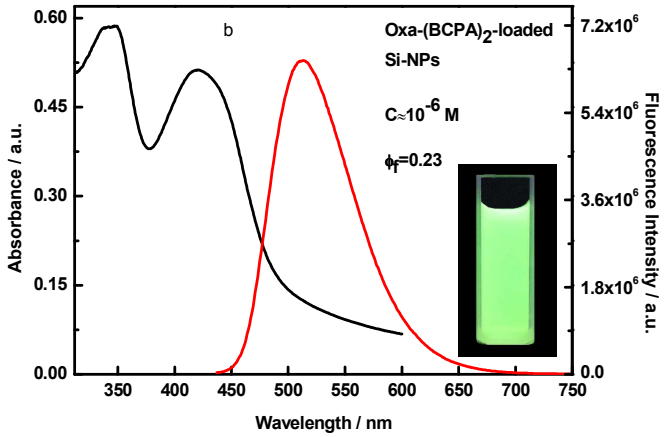

Fig. 8 Absorption and fluorescence spectra of SiO_2-NPs of Oxa-$(BCPA)_1$ (a) and Oxa-$(BCPA)_2$ (b) in water(10^{-6} M); the insets are fluorescence pictures of NPs in water excited at 365 nm.

Table 2 Photophysical properties of the four chromophores Oxa-(CPA)n and Oxa-$(BCPA)_n$ (n=1,2) in different aggregated states

	f_W=80%		f_W=90%		Si-NPs[a]	
	λ_{abs} (nm)	λ_{em} (nm) / Φ_f	λ_{abs} (nm)	λ_{em} (nm) / Φ_f	λ_{abs} (nm)	λ_{em} (nm) / Φ_f
Oxa-$(CPA)_1$	421	508 /0.28	405	501 /0.24	411	500 /0.13
Oxa-$(CPA)_2$	428	509 /0.08	430	506 /0.07	414	507 /0.07
Oxa-$(BCPA)_1$	417	515 /--	412	510 /0.53	419	476 /0.35
Oxa-$(BCPA)_2$	434	515 /--	439	509 /0.24	420	513 /0.23

* f_W water fraction of THF and water system; [a] Si-NPs dispersed in water; λ_{abs} UV absorption maximum; λ_{em} fluorescence emission maximum; Φ_f fluorescence quantum yield

Cell imaging

Dye-loaded BSA-NPs[17] were synthesized and investigated and the preparation process was presented in Fig. 9. With the THF solution of chromophores gradually added into the aqueous solution of BSA, the dye molecules aggregated because of its poor solubility in water and the aggregated molecules entangled with BSA chain. When the addition process finished, the mixture would be a mixed solvent of water and THF system of 38% (V/V) water fraction. Then glutaraldehyde (GA) was added to knit together the BSA matrix. After the reaction finished, the THF was removed and the mixture returned into aqueous system but BSA matrix would not be dissolved back into water because of the GA-knitted structure.

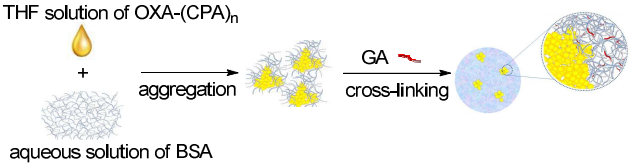

Fig. 9 The preparation process and model structure of dye-loaded BSA nanoparticles.

TEM image of the dye-loaded BSA-NPs are shown in Fig. 10. It indicates that the dye-loaded BSA-NPs have a spherical shape and a smooth surface.

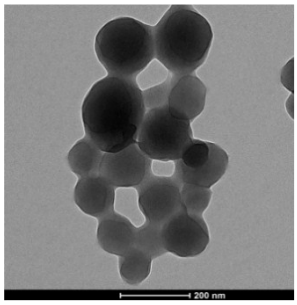

Fig. 10 TEM pictures of Oxa-$(BCPA)_2$.

Similar to the dye-doped Si-NPs, the chromophore molecules in the dye-loaded BSA-NPs were in aggregated states and thus the photophysical properties were kept due to AIE effect. BSA matrix was introduced to improve the bio-compatibility of the nanoparticles and to enhance the permeability and retention effect of the chromophores.

The dye-loaded BSA-NPs were incubated with HeLa cells for 4 hours at 37 ℃ and fixed for cell imaging and the result was presented in Fig. 11. From the imaging bright green fluorescence emitted from the chromophores could be clearly seen, which covered the cells very well. Compared with bare chromophore NPs, which were failed to be uptaken by HeLa cells in the same incubation conditions, dye-loaded BSA-NPs showed an excellent intracellular uptake and a high fluorescence contrast, which suggested dye-loaded BSA-NPs could be potential cancer cell biosensors with good biocompatibility and photostability. The cytotoxicity of the dye-loaded BSA-NPs against HeLa cells was investigated using a MTT cell-viability assay according to the known literature procedure.[17] High cell viabilities of more than 92% were observed, indicating low cytotoxicity of the dye-loaded BSA-NPs (Fig. S2).

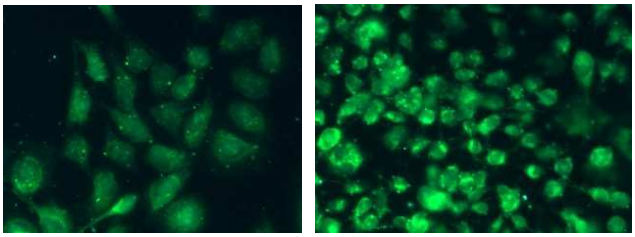

Fig. 11 Fluorescence imaging pictures of HeLa cells treated with dye-loaded BSA nanoparticles containing Oxa-$(BCPA)_1$ and Oxa-$(BCPA)_2$.

In this part, based on the excellent AIE properties and high quantum yield of the chromophores, the photophysical properties of dye-doped Si-NPs were investigated and high quantum up to 35% for Oxa-$(BCPA)_1$ and good dispersing ability in water for all the chromophores were observed. Dye-loaded BSA-NPs were also successfully applied to cell imaging.

Conclusions

With combination of carbazole-containing triphenylamine with 1,3,4-oxadiazole by conjugated π-bridge, two groups of aggregation-induced emission and intramolecular charge transfer active chromophores were synthesized. Strong structure-related emissions of the chromophores in solid states with peaks ranging from 494 nm to 523 nm were observed, showing an obvious change from green to yellowish green when the one-donor-containing compounds changed into two-donor-containing compounds. Remarkable solvatochromism effect was found and the emission peaks for Oxa-$(CPA)_1$ ranged from 498 nm in chloroform to 545 nm in DMF for instance.

Aggregation-induced emission and intramolecular charge transfer effect was also found in mixed solvent of water and THF system. Obvious bathochromic shifts was observed with the increase of the water fraction and the quantum yield in THF was up to 0.54 for Oxa-$(BCPA)_1$, for instance, while in mixed solvent of water and THF system with water fraction of 90%, the quantum yield was 0.53.

Based on the excellent performances of the chromophores in aggregated states, dye-loaded nanoparticles were prepared and tested. The dye-doped silica nanoparticles indicated that besides the greatly enhanced bio-compatibility, the inherent advantages of the pure dyes were also maintained and the quantum yield of Oxa-$(BCPA)_1$-doped silica nanoparticles was even up to 35%. Most importantly, it provided a promising approach in exploring applications in bioprobes by decorating the surface of the silica nanoparticles with different functional components. The dye-loaded BSA-nanoparticles were applied to cell imaging and showed a better uptake by HeLa cells compared to pure dye nanoparticles, which indicating dye-loaded BSA-nanoparticles could be significant biosensors in cancer cell detecting. The detailed bioapplications of these materials are underway.

Acknowledgements

We thank the financial support from the National Natural Science Foundation of China (Grant numbers: 60678042 and 61178057). We thank Prof. S. Q. Liu, Dr H. N. Li, D. H. Chen, Y. M. Zhang for their kind help with the cell culture and MTT assay.

Notes and references

1 (a) Xiaoyong Zhang, Xiqi Zhang, Shiqi Wang, Meiying Liu, Yun Zhang, Lei Tao and Yen Wei, *ACS Appl. Mater. Interfaces*, 2013, 5, 1943; (b) Xueling Zhao, Zongyan Chen, Hongli Zhao, Denghao Zhang,a Liang Tao and Minbo Lan, *RSC Adv.*, 2014, 4, 62153; (c) Xiaoyong Zhang, Xiqi Zhang, Bin Yang, Liangji Liu, Junfeng Hui, Meiying Liu, Yiwang Chen and Yen Wei, *RSC Adv.*, 2014, 4, 10060; (d) Henan Li, Yawen Mu, Jusheng Lu, Wei Wei, Yakun Wan and Songqin Liu, *Anal. Chem.* 2014, 86, 3602; (e) Marine Perrier, Magali Gary-Bobo, Lenaı¨c Lartigue, David Brevet, Alain More`re, Marcel Garcia, Philippe Maillard, *J Nanopart Res*, 2013, 15, 1602; (f) Babao Lin, Xiuzhong Yao, Yihua Zhu, Jianhua Shen, Xiaoling Yang and Chunzhong Li, Chiara Agnoletto, Giorgio Zauli and Paola Secchiero, *RSC Adv.*, 2014, 4, 20641; (g) Hongxing Xia, Xiaoquan Yang, Jitao Song, Jun

Chen, Mingzhen Zhang, Dongmei Yan, Lin Zhang, Mengyao Qin, Lingyu Bai, Yuan-di Zhao and Zhiya Ma, *J. Mater. Chem. B*, 2014, 2, 1945

2 (a) Xiaoting Yu, Xu Jia, Xiaolong Yang, Weisheng Liu and Wenwu Qin, *RSC Adv.*, 2014, 4, 23571; (b) Kasoju Aruna, T. Mohammad Munawar, M.V.Prashanthi,M.Lakshmi Narsu, *International Journal of Advanced Research*, 2013, 1, 1; (c) Raffaele Riccò, Anna Meneghello, Francesco Enrichi, *Biosensors and Bioelectronics*, 2011, 26, 2761; (d) Eue Soon Jang, Seung Yong Lee, Eui-Joon Cha, In-Cheol Sun, Ick Chan Kwon, Dukjoon Kim, Young II Kim, Kwangmeyung Kim and Cheol-Hee Ahn, *Pharm Res*, 2014, 31, 3371; (e) B Korzeniowska, R Nooney, D Wencel and C McDonagh, *Nanotechnology*, 2013, 24, 442002(20pp); (f) Vinoth Kumar Rajendran, Padmavathy Bakthavathsalam, Baquir Mohammed Jaffar Ali, *Microchim Acta*, 2014, 181, 1815

3 (a) Jianliang Shen, Hancheon Kim, Hua Su, Feng Wang, Joy Wolfram, Dickson Kirui, Junhua Mai, Chaofeng Mu, Liangnian Ji, Zongwan Mao, Haifa Shen, *Theranostics*, 2014, 4, 487; (b) Dechao Niu, Zuojin Liu, Yongsheng Li, Xiaofeng Luo, Junyong Zhang, Jianping Gong and Jianlin Shi, *Adv. Mater*. 2014, 26, 4947; (c) Sandy B Hartono, Meihua Yu, Wenyi Gu, Jie Yang, Ekaterina Strounina, Xiaolin Wang, Shizhang Qiao and Chengzhong Yu, *Nanotechnology*, 2014, 25, 055701 (12pp); (d) Fengpeng Chang, Linyun Kuang, Chia-An Huang, Wannneng Jane, Yann Hung, Yue-ie C. Hsing and Chungyuan Mou, *J. Mater. Chem. B*, 2013, 1, 5279; (e) Xing Ma, Yun Zhao, Kee Woei Ng and Yanli Zhao, *Chem. Eur. J*., 2013, 19, 15593; (f) Jiantao Lin, Chao Wang, Yi Zhao and Guanhai Wang, *Materials Research Express*, 2014, 1, 0354031

4 (a) S. Karthik, Avijit Jana, Biswajit Saha, B. Krishna Kalyani, Sudip Kumar Ghosh, Yanli Zhao and N. D. Pradeep Singh, *J. Mater. Chem. B*, 2014, 2, 7971; (b) Christophe Thron, Audrey Gallud, Carole Carcel, Magali Gary-Bobo, Marie Maynadier, Marcel Garcia, Jie Lu, Fuyuhiko Tamanoi, Jeffrey I. Zink and Michel Wong Chi Man, *Chem. Eur. J*., 2014, 20, 9372; (c) Rajendra K. Singh, Tae-Hyun Kim, Kapil D. Patel, Jung-Ju Kim and Hae-Won Kim, *J. Mater. Chem. B*, 2014, 2, 2039; (d) Rijun Gui, Yanfeng Wang, Jie Sun, *Colloids and Surfaces B: Biointerfaces*, 2014, 116, 518; (e) Bei Liu, Chunxia Li, Dongmei Yang, Zhiyao Hou, Ping'an Ma, Ziyong Cheng, Hongzhou Lian,Shanshan Huang and Jun Lin, *Eur. J. Inorg. Chem*., 2014, 1906; (f) Robert Roggers, Shrey Kanvinde, Suthida Boonsith and David Oupický, *AAPS PharmSciTech*, 2014, 15, 5; (g) Peng Zhang, Tianyi Wang, Huanming Xiong, Jilie Kong, *Talanta*, 2014, 127, 43

5 Jingdong Luo, Zhiliang Xie, Jacky W. Y. Lam, Lin Cheng, Haiying Chen, Chengfeng Qiu, Hoi Sing Kwok, Xiaowei Zhan, Yunqi Liu, Daoben Zhu and Ben Zhong Tang, *Chem. Commun.*, 2001, 1740

6 (a) Youyong Yuan, Ryan T. K. Kwok, Benzhong Tang and Bin Liu, *J. Am. Chem. Soc.,* 2014, 136, 2546; (b) Xiangdong Xue, Yuanyuan Zhao, Luru Dai, Xu Zhang, Xiaohong Hao, Chunqiu Zhang, Shuaidong Huo, Juan Liu, Chang Liu, Anil Kumar, Weiqiang Chen, Guozhang Zou and Xingjie Liang, *Adv. Mater.,* 2014, 26, 712

7 Zhengke Wang, Sijie Chen, Jacky W. Y. Lam, Wei Qin, Ryan T. K. Kwok, Ni Xie, Qiaoling Hu and Ben Zhong Tang, *J. Am. Chem. Soc.,* 2013, 135, 8238

8 Jie Zhao, Dong Yang, Yanxia Zhao, Xiao-Juan Yang, Yao-Yu Wang and Biao Wu, *Angew. Chem. Int. Ed.,* 2014, 53, 6632

9 Zilong Wang, Bin Xu, Lei Zhang, Jibo Zhang, Tenghe Ma, Jiabao Zhang, Xueqi Fu and Wenjing Tian, *Nanoscale*, 2013, 5, 2065

10 Jung Aa Ko and H. B. Lim, *J. Anal. At. Spectrom.*, 2013, 28, 630

11 Stefania Biffi, Luca Petrizza, Enrico Rampazzo, Rebecca Voltan, Massimo Sgarzi, Chiara Garrovo, Luca Prodi, Laura Andolfi, *RSC Adv.*, 2014, 4, 18278

12 Feng Gao, Peng Cui, Xiaoxiao Chen, Qingqing Ye, Maoguo Li and Lun Wang, *Analyst*, 2011, 136, 3973

13 Yun Xia, Min Li, Tao Peng, Weijie Zhang, Jun Xiong, Qinggang Hu, Zifang Song and Qichang Zheng, *Int. J. Mol. Sci.*, 2013, 14, 1080

14 (a) Binbin Wang and Ying Qian, New J. Chem.,2013, 37, 1402; (b) Ying Qian, Zhifeng Lu, Changgui Lu, Zhiming Chen, Yiping Cui, *Dyes and Pigments*, 2007, 75, 641; (c) Binbin Wang and Ying Qian, *Chin. J. Org. Chem.* 2014, 34, 210; (d) Xiaoqin Zhu and Ying Qian, *Chinese Journal of Organic Chemistry*, 2009, 29, 1975; (e) Hua Yang and Ying Qian, *Chin. J. Org. Chem.*, 2013, 33, 184; (f) Ying Qian, Xinming Lv, Zhiqing Zhou and Yiping Cui, *Chemical Journal of Chinese Universites*, 2011, 32, 2441; (g) Kaiming Hu and Ying Qian, *Actachimicasinica*, 2010, 68, 1; (h) Ying Qian, Manli Luo, *Dyes and Pigments*, 2014, 101, 240

15 Wei Huang, Fansheng Tang, Bo Li, Jianhua Sua and He Tian, *J. Mater. Chem. C*, 2014, 2, 1141

16 (a) Tinghua Xu, Ran Lu, Xingliang Liu, Xiangqian Zheng, Xianping Qiu, and Yingying Zhao, *Org. Lett.*, 2007, 9, 5; (b) Jiuyan Li, Ting Zhang, Yunjing Liang and Ruixia Yang, *Adv. Funct. Mater.* 2013, 23, 619

17 Wei Qin, Dan Ding, Jianzhao Liu, Wang Zhang Yuan, Yong Hu, Bin Liu and Ben Zhong Tang, *Adv. Funct. Mater.* 2012, 22, 771

18 Tainan Duan, Ke Fan, Cheng Zhong, Wuwei Gao, Xingguo Chen, Tianyou Peng, Jingui Qin, *Journal of Photochemistry and Photobiology A: Chemistry*, 2014, 278, 39

19 (a) Zhangyuan Wang, Yongyang Gong, Shuming Chen, et al, *Chem. Mater*. 2012, 24, 1518; (b) Yilin Li, Zhipeng Li, Yang Wang, *Energy Environ. Sci.*, 2013, 6, 2907; (c) Ziqi Yana, Zhiyong Yang, Hai Wang, *Spectrochimica Acta Part A*, 2011, 78, 1640; (d) Bingrong Gao, Haitu Wang, Yawei Hao, *J. Phys. Chem. B*, 2010, 114, 128

20 (a) J.S. Kadadevarmath, G.H. Malimath, N.R. Patil, *Can. J. Phys*., 2013, 91, 1107; (b) S. A. El-Daly, A. M. Asiri , K. A. Alamry, *J Fluoresc*, 2014, 24, 1307

21 (a) B.Z. Tang, Y. Geng, Lam JWY, B. Li, X. Jing, X. Wang, F. Wang, Pakhomov AB, X. Zhang, *Chem Mater*, 1999, 11, 1581; (b) Yuting Gao, Hao Zhang, Tao Jiang, Ji Yang, Bo Li, Zhen Li, *Sci China Chem*, 2013, 56, 1204

22 Peiyang Gu, Caijian Lu, Zhijun Hu, *J. Mater. Chem. C*, 2013, 1, 2599

23 Guofeng Zhang, Matthew P. Aldred, *Chem. Commun.*, 2012, 48, 7711

24 Chenfei Guan and Ying Qian, Chin. *J. Org. Chem.,* 2014, 34, 537

25 (a) Zhou Jiang, Tingting Yang, Minyan Liu, Yanli Hu and Jian Wang, *Biosensors and Bioelectronics*, 2014, 53, 340; (b) Sehoon Kim, Tymish Y. Ohulchanskyy, Dhruba Bharali, Yihui Chen, Ravindra K. Pandey and Paras N. Prasad, *J. Phys. Chem. C*, 2009, 113, 12641; (c) Zhivko Zhelev, Hideki Ohba and Rumiana Bakalova, *J. AM. CHEM. SOC*. 2006, 128, 6324

26 (a) Jun Qian, Xin Li, Ming Wei, Xiangwei Gao, Zhengping Xu and Sailing He, *Optics Express*, 2008, 16, 19568; (b) Xuhua Wang, Sheng Yao, Hyo-Yang Ahn, Yuanwei Zhang, Mykhailo V. Bondar, Joseph A. Torres and Kevin D. Belfield, *Biomedical Optics Express*, 2010, 1, 453

